

# *Selection and verification of the mathematical model and mesh of The GPSD under moving water condition*

**Ruiming Song<sup>1</sup>, Cheng Yin<sup>1,\*</sup>, Yong Yang<sup>1</sup>, Lan Zheng<sup>1</sup>, Weijian Ge<sup>2</sup>, Sunyou Hao<sup>1</sup>, Zhipeng Chen<sup>1</sup>, Gangbo Dong<sup>1</sup>, Lei Yu<sup>3</sup>**

<sup>1</sup>Anhui Water Conservancy Technical College, Hefei, Anhui, 231603, China

<sup>2</sup>Comenius University Bratislava, Bratislava, 85000, Slovakia

<sup>3</sup>Faculty of Management, Hefei University of Technology, Hefei, Anhui, 230001, China

\*Corresponding author

**Keywords:** Numerical simulation; computational methods; mathematical model; mesh; water-sand two-phase flow; Gill-piece separation device (GPSD)

**Abstract:** In order to ensure the accuracy of numerical simulation results for the Gill-piece separation device (GPSD), an exploration of the optimal mathematical model and mesh parameters was conducted. The Mixture model in CFX was coupled with RNG  $k-\varepsilon$ , SST, BSL, and SSG turbulence models to simulate the water-sand two-phase flow field in the GPSD under dynamic water conditions. By comparing the numerical simulation results with physical experimental phenomena, it is found that the velocity vector diagram calculated by the Mixture-RNG  $k-\varepsilon$  coupling model conforms more closely to the physical experimental phenomena (Double-layered Counterflow), and the relative error of the water-sand separation efficiency calculated by the Mixture-RNG  $k-\varepsilon$  coupling model is very small, only 1.77%. Thus, it can be regarded as the optimal mathematical model for numerical simulation of the GPSD under dynamic water conditions. Considering factors such as computational time, the number of mesh in numerical simulation should be set to around 300,000 for the best performance.

## 1. Introduction

The Gill-piece separation device (GPSD) is a novel water-saving irrigation tool primarily used for treating river water with viscous sand to prevent clogging of drip irrigation belts during agricultural irrigation processes[1]. Compared to conventional sand separation devices, the GPSD offers advantages such as rapid water-sand separation, small footprint, environmental friendliness, and low cost, thereby contributing to increased efficiency in agricultural water resource utilization[2,3]. Some experts and scholars have conducted preliminary experiments and studies on the GPSD, yielding relevant research findings: in a static water environment, the inclination angles  $\alpha$  and  $\beta$  of the gill-pieces are 60 °and 45 °respectively[4]; the channels for sand and clear water in the GPSD should be reasonably set, with a minimum diameter of 5mm[5]; different parameters such as sand content and flow rate have varying effects on the water-sand separation efficiency of the GPSD[6,7]; under static

water conditions, the greater the gill-pieces spacing is, the lower the water-sand separation efficiency is [8].

However, the internal flow field characteristics of the GPSD under dynamic water conditions and the effects of different parameters remain to be further investigated. In order to ensure the accuracy of numerical simulation results, prior to numerical simulation of the GPSD, the Mixture model in CFX was coupled with RNG, SST, BSL, and SSG turbulence models to conduct numerical simulation calculations of the GPSD [9]. The results were processed using Tecplot software, and through qualitative and quantitative comparisons, the optimal mathematical model and mesh quantity for numerical simulation of the GPSD under dynamic water conditions were explored. This lays a solid foundation and provides better technical support for future research on the GPSD.

## 2. Theory and Methods

### 2.1 Physical model

The physical model was constructed using the dimensions of the GPSD used in previous physical model experiments [10], as shown in Figure 1. The dimensions include: length (a), width (b), height (h), clear water channel, sand channel, diameter of turbid water inlet, diameter of clear water outlet, and diameter of sand discharge outlet, spacing between gill-pieces (d), longitudinal inclination angle, transverse inclination angle, which are 20cm, 10cm, 100cm, 1cm, 1cm, 5cm, 2cm, 2cm, 0.25cm, 60° and 45° respectively.

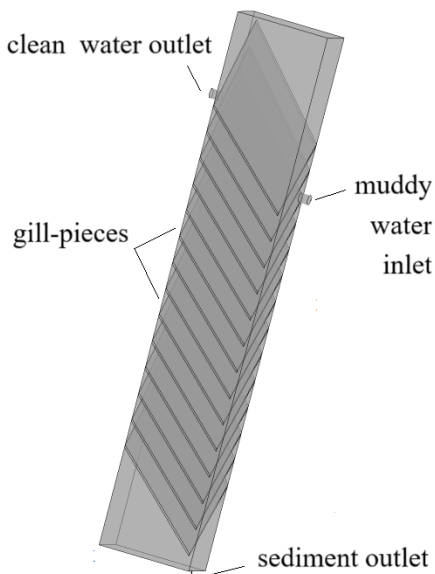


Figure 1: Three-dimensional geometric model diagram

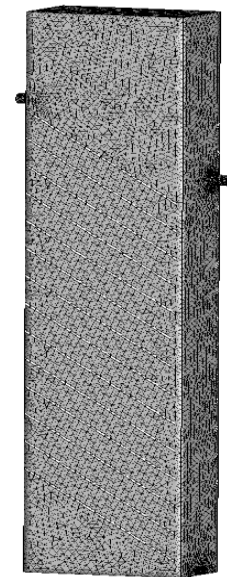


Figure 2: Computational mesh

### 2.2 Mesh

In numerical simulations, selecting the appropriate mesh type is crucial as well-matched mesh can enhance the accuracy and efficiency of numerical simulation results. For the GPSD in this experimental setup, its internal structure is relatively complex, particularly at the irregularities formed by the angle between the gill-pieces and the inner walls of the rectangular ducts. This irregularity poses challenges for mesh partitioning. Therefore, priority is given to using unstructured mesh for partitioning and tuning [11, 12], as shown in Figure 2.

## 2.3 The setting of initial conditions and boundary conditions

In the GPSD, the two media are water and sand. Therefore, in the CFX processor, water is set as the first phase (primary phase), with a relative volume fraction of 0.996. The second phase (secondary phase) is set as sand, with a relative volume fraction of 0.004, a density of 2650, and an average particle size of 0.025mm.

The boundary conditions set in the GPSD are as follows: (1) For the murky water inlet, it is set as a Velocity-inlet, with a flow rate of 0.9. (2) Both the water outlet and sand discharge outlet are set as Average Static Pressure-outlets. (3) For the solid wall surfaces, all entities are set as Walls.

## 2.4 Numerical Computation Methods and Mathematical Models

The basic governing equations for the GPSD and the discretization of the computational domain utilize the Finite Volume Method (FVM). Its advantages lie in the fact that within the entire computational domain, the results (such as momentum, energy, and mass) within any control volume can be accurately satisfied, while also demonstrating accurate integral balance for coarse mesh solutions. Finally, a multiphase flow model, namely the Mixture model is employed, coupled with four turbulence models (RNG  $k-\varepsilon$ , SST, BSL, SSG) within [13,14].

## 3. Numerical Computation Results Analysis

### 3.1 Comparison of Velocity Vector Distribution in the Transverse Direction for Different Coupling Models

In Figure 3, When the iteration terminates, the velocity vector distribution along the transverse direction ( $Y=0.4\text{dm}$ ) in the middle part of the GPSD is compared between different coupling models with the experimental phenomenon.

From Figure 3(a), it can be observed that the velocity streamlines downward on the upper surface of the gill-pieces are denser, indicating that sand particles gather along the upper surface of the gill-pieces to form a sand flow moving from the top left corner to the bottom right corner. Sand flows from different layers gather at the far right of the GPSD and move vertically downward in the sand channel. The dense upward velocity streamlines adjacent to the lower surface of the gill-pieces represent the upward movement of clean water, indicating that clean water gathers along the lower surface of the gill-pieces to form a clean water flow moving from the bottom right corner to the bottom left corner and converging at the far left of the GPSD, collectively moving upward. The velocity vector distribution of this coupling model matches the experimental phenomenon shown in Figure 3(e).

The flow patterns in Figure 3(b) and (c) are relatively similar. In the region near the high end of the gill-pieces channel (between the upper and lower gill-pieces), some sand diverges vertically upward on the upper surface of the gill-pieces, and the turbulence between the two gill-pieces is significant, with no clear manifestation of the double-layered flow. In Figure 3(d), it can be observed that near the upper left corner of the GPSD, most streamlines diverge diagonally downward along the lower surface, indicating downward movement of clean water, which does not correspond to the observed behavior of clean water movement in the physical experiment.

In summary, the results simulated by the Mixture-RNG  $k-\varepsilon$  coupling model better match the observed behavior in the physical experiment.

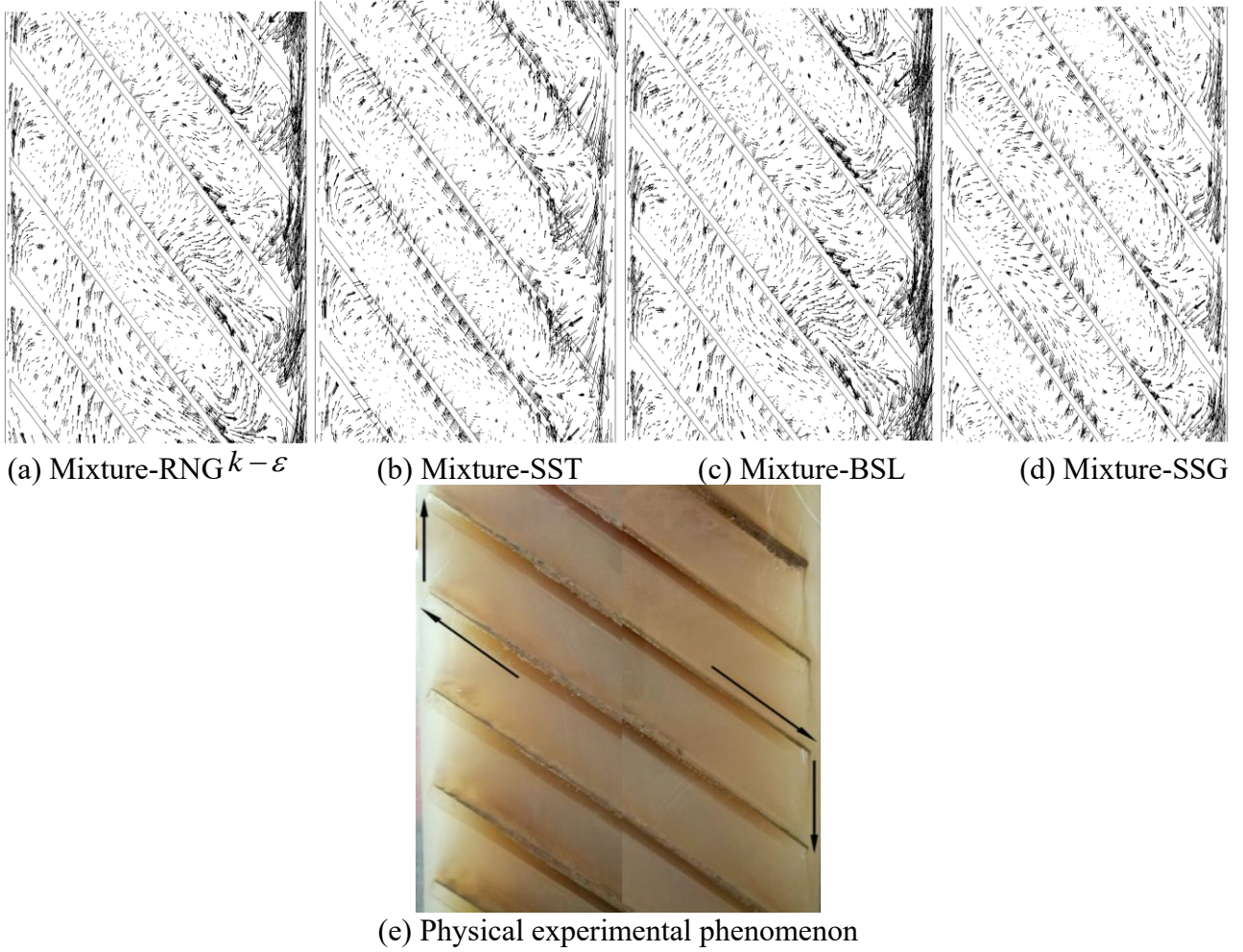


Figure 3:  $Y=0.4dm$  The velocity vector distribution of the cross-section and the physical experimental phenomenon

### 3.2 The water-sand separation efficiency and relative error of different coupling models.

#### 3.2.1 The water-sand separation efficiency of different models.

The numerical simulation concludes, extracting the average volume ratio of sand particles at the inlet section and the outlet section. Using Equation (1), the average sand concentration at these two sections is calculated. Then, according to Equation (2), the water-sand separation efficiency under different coupling models is obtained.

$$S_{\bar{h}} = \rho_s S_{\bar{m}} \quad (1)$$

$$\eta = \frac{S_{\bar{h}_i} - S_{\bar{h}_c}}{S_{\bar{h}_i}} \times 100\% \quad (2)$$

In the equation,  $\rho_s$  represents the density of sand, taken as  $\rho_s=2650\text{kg}/\text{m}^3$ ;  $S_{\bar{m}}$  represents the average volume ratio of sand particles at the target section;  $S_{\bar{h}}$  represents the average sand concentration at the target section, in  $\text{kg}/\text{m}^3$ ;  $\eta$  represents the water-sand separation efficiency

(numerical simulation), in %;  $S_{hj}$  represents the average sand concentration at the inlet section of murky water, in  $\text{kg}/\text{m}^3$ ;  $S_{hc}$  represents the average sand concentration at the outlet section of clean water, in  $\text{kg}/\text{m}^3$ .

In Table 1, at the termination of iteration, the average sand concentration at the inlet and outlet sections, as well as the water-sand separation efficiency obtained from numerical simulations, are presented for the four coupling models. From Table 1, it can be observed that due to the constant sand concentration set at the inlet of murky water, the average sand concentration at the inlet section for all four coupling models remains the same, at 10.00. However, the average sand concentration at the outlet section of clean water varies among the models, resulting in different water-sand separation efficiencies for each model.

Table 1: The average sand concentration and water-sand separation efficiency at the inlet and outlet sections for different mathematical models

Coupling models	Average sand concentration at the inlet section ( $\text{kg}/\text{m}^3$ )	Average sand concentration at the outlet section ( $\text{kg}/\text{m}^3$ )	Water-sand separation efficiency (%)
Mixture-RNG $k-\varepsilon$	10.00	6.55	34.50
Mixture-SST	10.00	7.92	20.79
Mixture-BSL	10.00	7.97	20.34
Mixture-SSG	10.00	7.73	22.71

### 3.2.2 Relative errors of different models

To determine the computational accuracy of each coupling model, the results of the four calculations are compared with the physical experiment, using relative error to represent the consistency, as expressed by Equation (3):

$$H = \left| \frac{\eta - n}{n} \right| \times 100\% \quad (3)$$

In the equation,  $H$  represents the relative error;  $\eta$  represents the water-sand separation efficiency obtained from numerical simulation;  $n$  represents the water-sand separation efficiency from the physical experiment.

Table 2 compares the relative errors between different mathematical models and the physical experiment. It can be observed that the relative error of the Mixture-RNG  $k-\varepsilon$  model is the smallest, below 5%. This is mainly attributed to the fluctuation of temperature in the physical experiment environment. On the other hand, the relative errors of the other three models are large, all exceeding 30%, indicating that the reliability of the Mixture-RNG  $k-\varepsilon$  model is higher.

Table 2: Comparison of relative errors between different mathematical models and physical tests

Coupling models	Numerical simulation	Physical experiment	Relative error (%)
	Water-sand separation efficiency (%)		
Mixture-RNG $k-\varepsilon$	34.50	35.12	1.77
Mixture-SST	20.79		40.80
Mixture-BSL	20.34		42.08
Mixture-SSG	22.71		35.33

In summary, qualitative and quantitative comparisons indicate that the Mixture model coupled with the RNG  $k-\varepsilon$  turbulence model is the optimal mathematical model for simulating the two-phase flow field of water and sand in a dynamic water condition within the GPSD.

### 3.3 Mesh Independence Analysis

#### 3.3.1 Comparison of velocity vector distributions for different numbers of meshes

The quantity of meshes is a pivotal factor in mesh partitioning, influencing the quality of post-processing, computational accuracy, and computational time. Therefore, three different mesh partitioning schemes were employed: Scheme 1 with a total of 171,600 meshes; Scheme 2 with a total of 304,800 meshes; and Scheme 3 with a total of 617,600 meshes. The post-processing of the calculation results was conducted in, with the same settings for line thickness, vector type mesh, and units/magnitude [15].

Figure 4 shows the velocity vector plots on the  $Y=0.34$  section for the three different mesh schemes. It can be observed from Figure 4 that the velocity vector density in Scheme 3 is too high. In Scheme 1, the velocity vector density is too low. Scheme 2, however, displays velocity vector streamlines more clearly, making it easier to observe.

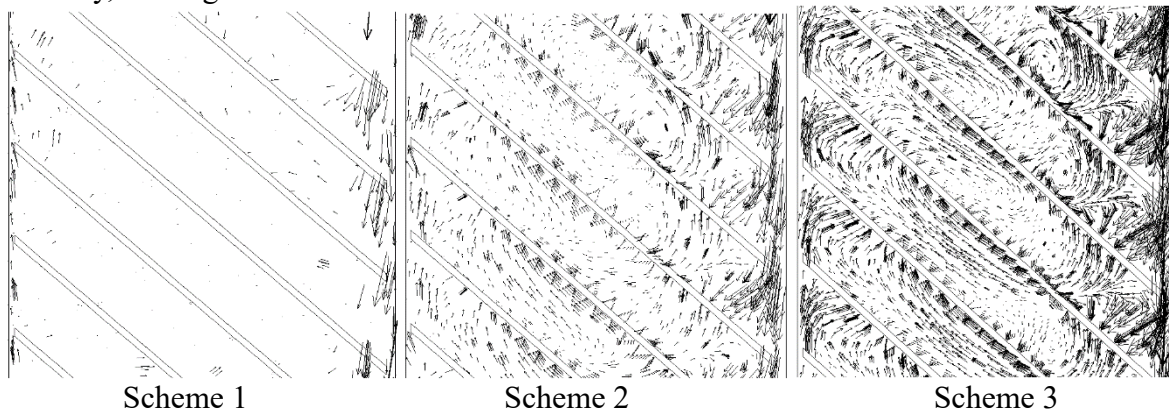


Figure 4: Velocity vector distribution maps for different numbers of meshes at the  $Y=0.34$ dm section

#### 3.3.2 Comparison of maximum sand velocity on the gill surface for different numbers of meshes.

Figure 5 illustrates a comparison of the maximum sand velocities on the surfaces of seven gill-pieces for three different mesh schemes. From Fig.5, it can be observed that the variation trend of the maximum sand velocity on the gill-pieces surfaces is consistent across the three mesh schemes, and the maximum sand velocities on the same gill-pieces are similar. Therefore, all three mesh schemes are feasible. For improving the accuracy of numerical simulation results, denser meshes are preferable. However, denser meshes result in longer computation times and higher demands on computer memory and processing power. Therefore, Scheme 2 may be preferred as it strikes a balance between computational accuracy and efficiency.

In summary, considering visualization quality, computational accuracy, and computational time, Scheme 2 is chosen as the final mesh partitioning scheme. This involves using unstructured meshes with a mesh count of 304,800.

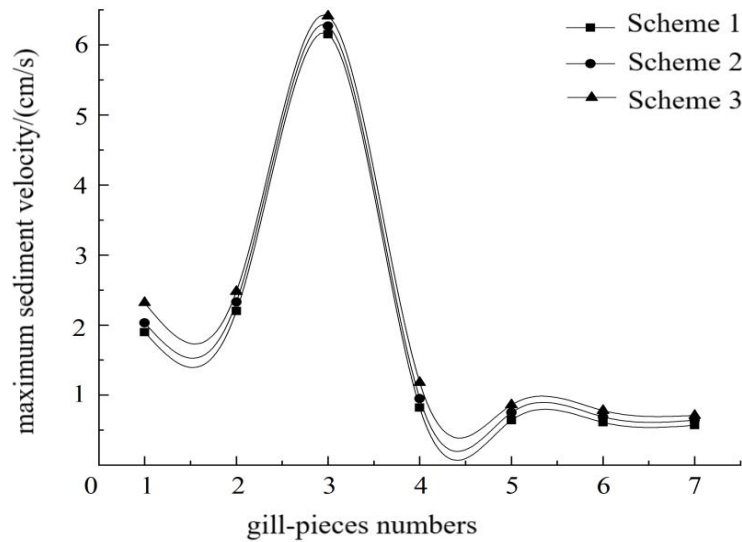


Figure 5: Maximum sand velocities on the surfaces of seven gill-pieces for different schemes

#### 4. Conclusion

1) The vector distribution maps obtained from the Mixture model and the RNG  $k-\varepsilon$  turbulence model are consistent with the phenomenon observed in the physical experiment. The streamline distribution in the vector distribution maps clearly demonstrates the presence of the double-layered flow patterns, making it the optimal mathematical model for simulating the two-phase flow field of water and sand within the GPSD under dynamic water conditions.

2) Quantitative comparison of the water-sand separation efficiency calculated by the four coupling models with the water-sand separation efficiency observed in the physical experiment reveals the relative errors. Among them, the relative error of the water-sand separation efficiency calculated by the Mixture-RNG  $k-\varepsilon$  coupling model is the smallest, at 1.77%, indicating high computational accuracy. The relative errors of the other three models are all above 35%.

3) Building upon this, a mesh independence analysis was conducted. By comparing the velocity vector maps and the maximum sand velocities on the gill-pieces surface for different numbers of meshand considering computational time, it was determined that the optimal number of meshfor simulating the GPSD under dynamic water conditions is approximately 300,000.

#### Acknowledgements

Project approval number: 2023AH053043 (Department of Education of Anhui Province)

#### References

- [1] Nabipour R, Yazdani R M, Mirzaei F, et al. Water productivity and yield characteristics of transplanted rice in puddled soil under drip tape irrigation [J]. *Agricultural Water Management*, 2024, 295108753.
- [2] Qiu Xiuyun, Gong Shouyuan, Yan Yuecheng, et al. (2007) Study on a New Type of Water-Sediment Separation Device. *Journal of sinkiang Agricultural University*, 30(01): 68-70.
- [3] Zhu Chao, Qiu Xiuyun. (2009) Experimental Study on Sediment Adaptability of the Vertical Counterflow GPSD. *Yangtze River*, 40(05): 60-61.
- [4] Zhu Chao, Qiu Xiuyun, Sun Xin. (2009) Experimental Study on the Effect of Baffle Inclination Angle on Sediment-water Separation in the GPSD. *Yellow River*, 31(10): 86-87.
- [5] Yan Yuecheng, Qiu Xiuyun, Zhang Xiang, et al. (2011) Experimental Study on the Influence of Width of Sedimentation Channel on Sediment-water Separation in the Two-phase Flow GPSD. *Journal of sinkiang Agricultural University*, 34(06):

526-528.

- [6] Luo Fei, Qiu Xiuyun, Li Lin. (2011) *Three-dimensional Numerical Simulation of Solid-liquid Two-phase Flow Field in the Single Baffle GPSD*. *Journal of Sinkiang Agricultural University*, 34(03): 77-80.
- [7] Luo Fei, Jiang Quanquan, Guo Hua, et al. (2012) *Numerical Simulation of Three-dimensional Flow Field in the Single Baffle GPSD with Inlet and Outlet Flow*. *Journal of Water Resources and Water Engineering*, 23(03): 253-258.
- [8] Tao Hongfei, Qiu Xiuyun, Li Qiao, et al. (2014) *Numerical Simulation of Three-dimensional Flow Field in the GPSD with Different Baffle Spacing*. *Transactions of the Chinese Society for Agricultural Machinery*, 45(6): 183-189.
- [9] Tao Hongfei, Qiu Xiuyun, Li Qiao, et al. (2015) *Numerical Simulation of Three-dimensional Flow Field in the GPSD with Different Inclination Angles of Baffle*. *Hydroelectric Energy Science*, 33(01): 157-161.
- [10] Zhang Jiling, Tao Hongfei, Li Qiao, et al. (2019) *Analysis of Sediment-water Separation Efficiency of the GPSD under Dynamic Water Conditions*. *Water-saving Irrigation*, (05): 41-45
- [11] Farshad K, Javad B, Vahid R, et al. *Field evaluation and numerical simulation of water and nitrate transport in subsurface drip irrigation of corn using HYDRUS-2D*[J]. *Irrigation Science*, 2023, 42(2):327-352.
- [12] Jafar C, Md H A. *Numerical simulation of pollution transport and hydrodynamic characteristics through the river confluence using FLOW 3D*[J]. *Water Supply*, 2022, 22(10):7821-7832.
- [13] V. P B, V. N P, O. L V. *Comparison of Turbulence Models in the Numerical Simulation of the Model Ducted Propeller*[J]. *Russian Aeronautics*, 2023, 65(4):713-721.
- [14] Z.M. M, M.E. M. *Numerical simulation of separated flow past a square cylinder based on a two-fluid turbulence model*[J]. *Journal of Wind Engineering Industrial Aerodynamics*, 2022, 231
- [15] Yifan B, Han W, Minyun L, et al. *Direct numerical simulation of flow and heat transfer of supercritical water with different heat fluxes*[J]. *International Journal of Heat and Mass Transfer*, 2024, 221125132.